Journal of Biomechanics 46 (2013) 1604–1610

Contents lists available at SciVerse ScienceDirect

Journal of Biomechanics

journal homepage: www.elsevier.com/locate/jbiomech
www.JBiomech.com

Evaluation of hyperelastic models for the non-linear and non-uniform high strain-rate mechanics of tibial cartilage

Jessica M. Deneweth [a,b,*], Scott G. McLean [a], Ellen M. Arruda [b,c,d]

[a] School of Kinesiology, University of Michigan, Ann Arbor, MI 48109, USA
[b] Department of Mechanical Engineering, University of Michigan, Ann Arbor, MI 48109, USA
[c] Department of Biomedical Engineering, University of Michigan, Ann Arbor, MI 48109, USA
[d] Program in Macromolecular Science & Engineering, University of Michigan, Ann Arbor, MI 48109, USA

ARTICLE INFO

Article history:
Accepted 15 April 2013

Keywords:
Constitutive modeling
Cartilage
Hyperelastic
Eight-chain network
Knee

ABSTRACT

Accurate modeling of the high strain-rate response of healthy human knee cartilage is critical to investigating the mechanism(s) of knee osteoarthritis and other cartilage disorders. Osteoarthritis has been suggested to originate from regional shifts in joint loading during walking and other high strain-rate physical activities. Tibial plateau cartilage under compression rates analogous to walking exhibits a non-linear and location-dependent mechanical response. A constitutive model of cartilage that efficiently predicts the non-linear and non-uniform high strain-rate mechanics of tibial plateau cartilage is important for computational studies of osteoarthritis development. A transversely isotropic hyperelastic statistical chain model has been developed. The model's ability to simulate the 1-strain/s unconfined compression response of healthy human tibial plateau articular cartilage has been assessed, along with two other hyperelastic statistical chain models. The transversely isotropic model exhibited a superior fit to the non-linear stress–strain response of the cartilage. Furthermore, the model maintained its predictive capability after being reduced from four degrees of freedom to one. The remaining material constant of the model, which represented the local collagen density of the tissue, demonstrated a regional dependence in close agreement with physiological variations in collagen density and cartilage modulus in human knees. The transversely isotropic eight-chain network of freely jointed chains with a regionally-dependent material constant represents a novel and efficient approach for modeling the complex response of human tibial cartilage under high strain-rate compression. The anisotropy and microstructural variations of the cartilage matrix dictate the model's response, rendering it directly applicable to computational modeling of the human knee.

1. Introduction

Deterioration of knee articular cartilage (AC) leads to severe joint debilitation in the form of osteoarthritis (Buckwalter et al., 2005). Identifying the mechanism(s) that causes healthy AC to degenerate into this diseased state is of high priority. While computational knee models enable the systematic and controlled evaluation of potential osteoarthritis disease mechanisms (Wilson et al., 2005), the utility of these models' results relies on the accuracy of the modeled AC.

Articular cartilage poses a modeling challenge due to its complex physiology and equally complex mechanical response. It consists of a solid phase of cartilage cells (chondrocytes) embedded within an extracellular matrix and a fluid phase of water and soluble ions (Poole et al., 2001). The extracellular matrix is composed mainly of cross-linked type II collagen fibrils and negatively charged proteoglycan macromolecules. The interaction of the solid and fluid phases creates a non-linear poroviscoelastic response to compressive loading (Mow et al., 1984). Extensive work has been done to model this behavior (Boschetti et al., 2006; Hayes et al., 1972; Lai et al., 1991; Mak, 1986; Wilson et al., 2004). The short-term, high strain-rate response of AC, however, depends predominantly on the flow-independent, intrinsic viscoelasticity of the matrix (Bader and Kempson, 1994), which results from the collagen meshwork and its entrapment of high-swelling aggrecan macromolecules (Maroudas, 1976). The collagen network in the superficial tangential zone (STZ) is particularly important in the tissue's response to high-rate loading (Mizrahi et al., 1986). These data suggest that the mechanical response of knee AC to high-rate loading (e.g., walking) (Liu et al., 2010) may be represented by using the collagen meshwork and its anisotropy as the main input parameters. This unique approach would afford representation of the non-linear elastic response of AC with a low number of

* Correspondence to: 401 Washtenaw Avenue, Ann Arbor, MI 48109, USA. Tel.: +1 248 568 6369; fax: +1 734 764 5237.
E-mail address: jmden@umich.edu (J.M. Deneweth).

0021-9290/$ - see front matter © 2013 Elsevier Ltd. All rights reserved.
http://dx.doi.org/10.1016/j.jbiomech.2013.04.014

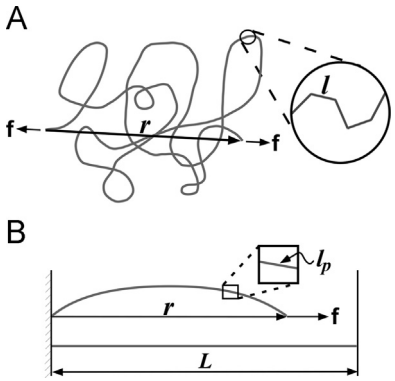

Fig. 1. Schematics of the two statistical chain models used to model tibial cartilage. The application of tension, *f*, stretches the chain to vector length *r*. (A) The highly flexible freely jointed chain, composed of *N* rigid links of length *l*. (B) The semi-flexible MacKintosh chain with contour length *L* and persistence length l_p. Adapted from Palmer and Boyce (2008).

material constants to facilitate implementation in a whole-joint computational model.

The structural properties of the STZ are non-uniform across the tibial plateau, which in turn may promote heterogeneous mechanical properties. The regions of the plateau covered by meniscal tissue, for example, tend to have a thicker STZ, more tangentially oriented collagen fibrils, and a higher collagen density, compared to regions not covered by meniscal tissue (Clark, 1991; Eyre et al., 2006). Individual collagen fibrils are primarily tensile elements. Thus when the collagen network is compressed, fibrils oriented perpendicular to the loading axis will stretch and resist the deformation, while fibrils oriented parallel to the loading axis will provide minimal load support. Therefore, regions with large amounts of tangentially oriented collagen fibrils, such as meniscus-covered regions, are expected to exhibit larger compressive stiffness compared to other regions, which has been supported experimentally (Barker and Seedhom, 2001; Shepherd and Seedhom, 1999; Young et al., 2007). The regional variability, however, may be more complex; we recently demonstrated that AC elastic moduli beneath the external and posterior portions of the menisci exceeded 300% of AC not covered by the meniscus and of AC beneath the anterior third of the menisci (Deneweth et al., 2013). Insight into knee AC behavior and the development of osteoarthritis, therefore, appear better served by modeling both the non-linear and non-uniform elastic response of the STZ.

Statistical mechanics models offer the ability to predict finite deformations of hyperelastic materials with relatively few material constants (Boyce and Arruda, 2000). These mechanistic models are particularly powerful because they offer insight into the underlying physiological factors driving mechanical behaviors (Ma et al., 2010). A material is represented as a cross-linked network of flexible molecular chains (Arruda and Boyce, 1993). The chains, which can be analogized to "entropy springs," produce significant forces when stretched but have minimal resistance to compression, much like collagen fibrils. As the material is deformed, the chains rotate and stretch to accommodate the deformation, altering the statistical entropy of the chain network and producing network stress.

Statistical mechanics models have accurately modeled multiple finite deformation states in elastic polymers (Boyce and Arruda, 2000; Boyce et al., 1994) and, more recently, in biological materials (Bischoff et al., 2004; Ma et al., 2010; Palmer and Boyce, 2008). Since the driver of knee AC short-term response, the collagen network, can be analogized to a statistical chain network, these models are strong candidates for modeling the short-term response of AC (Brown et al., 2009). However, the ability of the model to replicate the high strain-rates associated with walking or the non-uniform mechanical properties of tibial AC remains unknown. The purpose of this study, therefore, was two-fold. Firstly, the aim was to determine which, if any, of three popular statistical mechanics models could successfully model unconfined axial compression behavior of tibial AC, and secondly, to determine the extent to which the model that best fit the data could capture the regional mechanical properties of the tissue.

2. Methods

Statistical mechanics models have two key components: the mathematical description of the chains and the manner in which the chains are assembled to form a network. Two chain models, the freely jointed chain (FJC) model (Kühn and Grun, 1942) and the MacKintosh chain (MAC) model (MacKintosh et al., 1995), were each implemented within an isotropic eight-chain network (Arruda and Boyce, 1993; Palmer and Boyce, 2008). Additionally, the freely jointed chain was placed in a transversely isotropic eight-chain network (Bischoff et al., 2002) to develop a third model (TI). These three models were applied to experimental data from a series of unconfined axial compression tests of healthy human proximal tibial AC (Deneweth et al., 2013). The model that was found to best approximate the experimental data was further examined to determine the extent to which its parameters manifested regional dependence similar to that identified experimentally.

2.1. Freely jointed chain

The freely jointed chain is a highly flexible unconstrained rotating chain comprised of *N* rigid segments of length *l* positioned in three-dimensional space to give an initial chain vector length r_0 (Fig. 1a) (Kühn and Grun, 1942). The chain is highly flexible such that $r_0 \ll Nl$. Tension in the chain at length *r* is:

$$f_{FJC} = \frac{k\Theta}{l}\frac{r}{Nl}\frac{\left(3-\left(\frac{r}{Nl}\right)^2\right)}{\left(1-\left(\frac{r}{Nl}\right)^2\right)} \tag{1}$$

where *k* is Boltzmann's constant, $1.38065\times10^{-23}\,\mathrm{J\,K^{-1}}$, and Θ is the absolute temperature.

2.2. MacKintosh chain

The MacKintosh chain describes a semi-flexible statistical chain with significant bending rigidity. The length of the chain over which it appears straight, that is, its persistence length l_p, is approximately equal to its contour length *L* (Fig. 1b) (MacKintosh et al., 1995). The chain exhibits an average end-to-end resting length r_0 and an average vector length under no applied tension $r_{f=0}$. *L*, l_p, and $r_{f=0}$ are related by (Palmer and Boyce, 2008):

$$r_{f=0} = L\left(1-\frac{L}{6l_p}\right) \tag{2}$$

The tension developed in the chain when it is extended to an end-to-end length *r* can be written as:

$$f_{chain} = \frac{k\Theta}{l_p}\left(\frac{1}{4(1-r/L)^2}\right)\left(\frac{L/l_p-6(1-r/L)}{L/l_p-2(1-r/L)}\right) \tag{3}$$

2.3. Isotropic eight-chain network (FJC and MAC)

The isotropic eight-chain network treats a unit cell of material as a cube with sides aligned along the principal axes of stretch (Fig. 2) (Arruda and Boyce, 1993). Eight chains originate from the center of the cube and extend to each corner. Incorporating Eq. (1) into the isotropic eight-chain network yields the strain energy, U_{FJC}, for the FJC model:

$$U_{FJC} = nk\Theta N\left\{\frac{\lambda_{chain}}{\sqrt{N}}\beta_{chain} + ln\frac{\beta_{chain}}{sinh\beta_{chain}}\right\} \tag{4}$$

where *n* is the chain density, $\lambda_{chain} = (\lambda_1^2+\lambda_2^2+\lambda_3^2)^{1/2}/\sqrt{3}$, λ_i is the principal stretch in the *i*th direction ($i=1, 2, 3$), and β_{chain} is the inverse Langevin ($\mathscr{L}^{-1}$) of $\lambda_{chain}/\sqrt{N}$ (Arruda and Boyce, 1993).

Cartilage behaves as a nearly incompressible material under high strain-rates (Wong et al., 2000) and is frequently modeled as incompressible (Ateshian et al., 2007; Brown et al., 2009; Mow et al., 1980). For unconfined compression of an incompressible material, employing the Padé approximation of the inverse Langevin (Cohen, 1991), the nominal stress in the axial direction becomes (Arruda and Boyce, 1993):

$$T_{o1FJC} = \frac{nk\theta}{3}\frac{\sqrt{N}}{\lambda_{chain}}\mathscr{L}^{-1}\left(\frac{\lambda_{chain}}{\sqrt{N}}\right)(\lambda-1/\lambda^2) \tag{5}$$

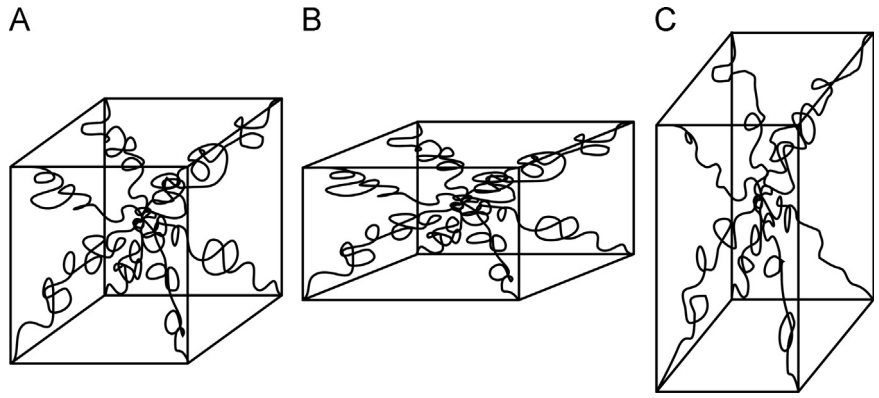

Fig. 2. Eight-chain isotropic network model (a) undeformed, (b) in unconfined compression, and (c) in uniaxial tension. The chains rotate and stretch to accommodate each deformation state. Adapted from Arruda and Boyce (1993).

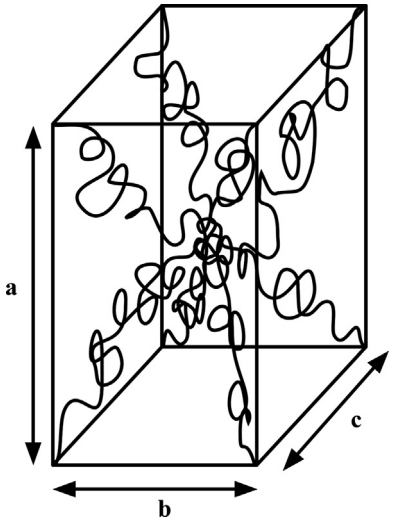

Fig. 3. Schematic of the eight-chain orthotropic network model. The unequal dimensions *a*, *b*, and *c* produce an anisotropic deformation response that is stiffest in the direction of the largest dimension. Adapted from Bischoff et al. (2002).

where λ is the applied axial stretch and $\lambda_{chain} = \left[(\lambda^2 + 2/\lambda)/3\right]^{1/2}$. The stress response depends on two material constants: $C_R = nk\theta$, an independent parameter that reflects the chain density per unit volume of the material, and N, a second independent parameter that is related to the chain contour length.

Similarly, the MAC strain energy is defined as (Palmer and Boyce, 2008):

$$U_{MAC} = nk\Theta\left\{\frac{L}{4l_p y} + \ln(y) - \ln(L - 2l_p y)\right\} \tag{6}$$

$$y = 1 - \frac{r}{L} = 1 - \frac{r_0 \lambda_{chain}}{L} \tag{7}$$

where n, k, Θ and λ_{chain} are defined identically to the FJC model. Assuming $r_0 = r_{f=0}$, the axial nominal stress is:

$$T_{o_1 MAC} = \frac{nk\Theta}{3l_p}\frac{r_{f=0}}{\lambda_{chain}}\left[\frac{1}{4(1 - r_{f=0}\lambda_{chain}/L)^2}\right]\left[\frac{L/l_p - 6(1 - r_{f=0}\lambda_{chain}/L)}{L/l_p - 2(1 - r_{f=0}\lambda_{chain}/L)}\right](\lambda - 1/\lambda^2) \tag{8}$$

Since $r_{f=0}$ is a function of l_p and L (Eq. (2)), the response depends on only three material constants: $C_R = nk\theta$, l_p, and L.

2.4. Freely jointed chain - transversely isotropic eight-chain formulation (TI)

An orthotropic eight-chain network was developed to simulate the anisotropic nonlinear behavior of soft tissue (Bischoff et al., 2002). The model incorporates orthotropic anisotropy into the traditional eight-chain framework by replacing the cubic unit cell with a rectangular prism of unequal, unitless sides a, b and c (Fig. 3). The material will exhibit the highest tensile modulus in the direction of the largest dimension. The total strain energy of the orthotropic eight-chain configuration of freely jointed chains, U_{Ortho}, is (Bischoff et al., 2002):

$$U_{Ortho} = U_0 + \frac{nk\Theta}{4}\left(N\sum_{i=1}^{4}\left[\frac{\rho^{(i)}}{N}\beta_\rho^{(i)} + ln\frac{\beta_\rho^{(i)}}{sinh\,\beta_\rho^{(i)}}\right] - \frac{\beta_P}{\sqrt{N}}ln\left[\lambda_{\mathbf{a}}^{a^2}\lambda_{\mathbf{b}}^{b^2}\lambda_{\mathbf{c}}^{c^2}\right]\right) + \frac{B}{\alpha^2}\{cosh[\alpha(J-1)] - 1\} \tag{9}$$

where U_0 is a constant; $\beta_\rho^{(i)} = \mathscr{L}^{-1}(\rho^{(i)}/N)$ and $\beta_P = \mathscr{L}^{-1}(P/N)$, where $P = \frac{1}{2}\sqrt{a^2 + b^2 + c^2} = \sqrt{N}$ is the undeformed chain length and $\rho^{(i)}$ is the deformed length of the ith chain; λ_{a-c} are the stretches along the principal material axes; J is the ratio of the deformed volume to the original volume, B controls the bulk compressibility near $J = 1$; and α is a constant that governs the curvature of the hydrostatic pressure versus volume curve for large volume changes.

The orthotropic model was simplified to one that more closely represented the physiology of the STZ, which dictates the short-term mechanical response (Mizrahi et al., 1986). The alignment of STZ collagen fibers primarily parallel to the AC surface (Bullough and Goodfellow, 1968) suggested that the STZ exhibits transverse isotropy (Askew and Mow, 1978). The orthotropic configuration was simplified to a transversely isotropic model by setting the in-plane dimensions b and c equal to one another and assuming that the stretches in these two principal directions are equal (i.e., $\lambda_b = \lambda_c = \lambda_2$). Small volume changes ($\alpha \cong 1$) were assumed to agree with the near incompressibility of the tissue (Wong et al., 2000). Therefore, for unconfined compression of the nearly incompressible transversely isotropic freely jointed eight-chain (TI) model, the nominal axial stress is:

$$T_{0_1 TI} = \frac{nk\theta}{4\lambda_1}\left(a^2\left[\frac{\lambda_1^2\beta_\rho}{\rho} - \frac{\beta_P}{\sqrt{N}}\right] - b^2\left[\frac{\lambda_2^2\beta_\rho}{\rho} - \frac{\beta_P}{\sqrt{N}}\right]\right) \tag{10}$$

where $\rho = \frac{1}{2}\sqrt{a^2\lambda_1{}^2 + 2b^2\lambda_2{}^2}$, $P = \sqrt{N} = \frac{1}{2}\sqrt{a^2 + 2b^2}$, and $\lambda_2 = \sqrt{J/\lambda_1}$. Four material constants are required: $C_R = nk\theta$; a, the unit cell dimension along the direction of compression (1-direction); b, the unit cell dimension perpendicular to the direction of compression (2-directions); and J.

Table 1
Demographic data for knee specimens.

Specimen	Side	Age (years)	BMI (kg/m^2)	Cause of death
1	Left	52	19	Cancer, appendix
2	Right	44	18	Neurofibrosarcoma
3	Right	51	19	Cancer, lung
4	Left	52	20	Cancer, unspecified
5	Left	54	14	Cancer, small bowel
6	Right	49	14	Cancer, breast
7	Right	51	16	Cancer, lung

2.5. Experimental data

To examine the effectiveness of the FJC, MAC, and TI formulations for modeling high strain-rate tibial AC behavior, experimental data were obtained from a separate study (Deneweth et al., 2013) in which non-osteoarthritic full-thickness AC samples were compressed at 1 strain/s from 0% to 20% nominal strain to replicate deformation during walking (Liu et al., 2010). Samples were extracted from 21 tibial plateau locations on each of eight female Caucasian knees [mean (standard deviation) age: 50 (3) years, and BMI: 17 (2) kg/m^2, Table 1]. The axial nominal stress–strain curves were used in the present study.

2.6. Determination of best fitting model

The three models were implemented in Matlab (Mathworks, Natick, MA). The unknown material constants were determined for each model using a built-in numerical nonlinear optimization scheme to minimize the squared difference between the model-predicted stress and the observed experimental stress (Coleman and Li, 1996). The unknown parameters were C_R and N for the FJC model; C_R, l_p, and L for MAC; and C_R, a, b, and J for TI. All parameters were constrained to be nonnegative as they represented lengths, moduli, or a volume ratio. Additional constraints to the TI model were $0.05 \le a:b \le 20$ with $a,b \ge 1$ to agree with experimentally determined anisotropy (Jurvelin et al., 2003; Wang et al., 2003; Woo et al., 1976) and $J \le 1$ (Chegini and Ferguson, 2010; Korhonen et al., 2002).

To determine the most successful model, the final experimental trial for each sample was submitted to the three model optimization schemes. Goodness of fit was calculated as:

$$R^2 = 1 - \frac{\sum_i (\sigma_{exp_i} - \sigma_{predi})^2}{\sum_i (\sigma_{expi} - \overline{\sigma}_{pred})^2}$$

where σ_{expi} is the experimental stress corresponding to the ith strain data point, σ_{predi} is the ith predicted stress, and $\overline{\sigma}_{pred}$ is the mean predicted stress.

2.7. Analysis of regional dependence

The formulation with the highest mean R^2 was used to evaluate whether it could predict location-specific dependence via the parameter C_R. The model was modified such that all parameters except C_R were assumed constant across the tibial surface. This adjustment was made to isolate the effect of C_R and to evaluate the viability of the simplest version of the model. The values of the fixed model parameters were determined from the results of the first set of simulations. The modified model was simulated against all available data trials using the same non-linear optimization scheme described above and evaluated via R^2.

Regional heterogeneity of C_R was evaluated by dividing the medial and lateral tibial plateaus into four regions: not covered by meniscus (I), and the anterior (II), exterior (III) and posterior (IV) thirds of the meniscus-covered area (Deneweth et al., 2013) (Fig. 4). The mean regional values of each parameter were submitted to a repeated-measures mixed model analysis of variance (ANOVA) to test for the effects of plateau side (medial or lateral, $n=2$), region ($n=4$), and the interaction of side × region ($n=8$) in SAS 8.0 (SAS Institute Inc., Cary, NC). Bonferroni-adjusted pairwise comparisons were made for all main effects. The effect size of each pairwise comparison was evaluated using Cohen's d (Cohen, 1988) to assess clinical relevance:

$$d_{AB} = \frac{\overline{X}_B - \overline{X}_A}{s_P}$$

where d_{AB} is the effect size between Regions A and B for the parameter of interest, $\overline{X}_J$ is the mean value of the parameter for Region J, and s_p is the pooled standard deviation of Regions A and B:

$$s_P = \sqrt{\frac{s_A^2(n_A - 1) + s_B^2(n_B - 1)}{n_A + n_B}}$$

The values of 0.2, 0.5, and 0.8 denote the cut-off levels of d for small, moderate, and strong effect sizes, respectively (Cohen, 1988). Only simulations with $R^2 \ge 0.97$ were included in the statistical analyses. Significance for all statistical measures was denoted by an alpha level of 0.05.

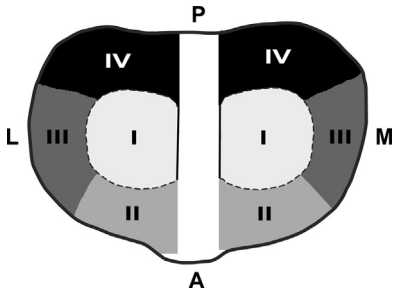

Fig. 4. For regional analysis, the tibial plateau was divided into the medial (M) and lateral (L) compartments. Each compartment was divided into four regions: I—not covered by meniscus and II–IV— anterior, exterior, and posterior one-thirds of the meniscus-covered area, respectively.

3. Results

3.1. Determination of best fitting model

C_R demonstrated the highest variability of the parameters across all simulations, while the values of the other parameters remained relatively constant (Table 2). The MAC configuration performed poorly ($R^2=0.900$, Table 1, Fig. 5). FJC and TI, in contrast, provided excellent model fits across the entire data set ($R^2=0.995$ and 0.999, respectively) (Table 2, Fig. 5). FJC and TI fit the small subset of linear stress–strain responses equally well (Fig. 5A). However, TI was superior in fitting the non-linear stress–strain curves of the majority (Fig. 5B). It was concluded that the TI model best captured the tibial AC stress–strain response, and it was used for subsequent analyses.

3.2. Analysis of regional dependence

The TI model was modified such that a and b were fixed at representative values of 1.00 and 1.33, respectively, based on the low variation in a and b in the first set of simulations (Table 2). Additionally, AC was assumed to be incompressible such that $J=1.00$. Implementing the TI model with $a=1.00$, $b=1.33$, and $J=1.00$ produced a good fit to the data ($R^2=0.983$, Fig. 5). Twelve percent of the simulations were excluded for $R^2 < 0.970$. The mean values of C_R for the remaining simulations are reported in Table 3.

A significant main effect on C_R was found for Region ($F(3,17)=11.16$, $p<0.001$, Fig. 6). A pairwise comparison of mean C_R by Region revealed significant differences ($p<0.05$) between Regions I and III, I and IV, II and III, and II and IV (Fig. 6, Table 4). The relative pattern of variability across regions was similar across subjects (Fig. 7). The mean difference of C_R between each pair of regions exhibited moderate to strong effect sizes except for I–II and III–IV on the lateral plateau and III–IV on the medial plateau (Table 4).

No significant main effect of Side was determined ($F(1,6)=3.12$, $p=0.13$), which indicated that mean C_R was statistically the same between the medial and lateral plateaus (Fig. 6). The small effect size between the medial and lateral plateaus ($d=0.32$) confirmed this finding. No statistically significant interaction of Region and Side was determined ($F(3,14)=0.55$, $p=0.65$).

4. Discussion

Three common statistical chain network models were evaluated to determine whether these formulations could represent the non-linear, non-uniform elastic response of healthy human tibial AC to a compression rate consistent with walking. Successful use of computational models to investigate the underlying mechanisms of osteoarthritis development can be enhanced by a constitutive model that reflects physiologically relevant human AC behavior with a minimal number of physically-meaningful material constants (Keenan et al., in press). The results of this study suggested the transversely isotropic eight-chain network with freely jointed chains (TI) appears to be such a model.

The TI model successfully simulated a wide range of tibial plateau AC responses (Deneweth et al., 2013). Moreover, its material constants (C_R, a, b, and J) and inherent anisotropy accurately represented AC physiology, which provides insight into the relationship between physiology and mechanics. Physiologically, C_R represents collagen density and mechanically dictates the initial slope of the stress–strain response and influences its tangent modulus. C_R may also reflect the integrity of the collagen matrix, with decreased values indicating a reduced amount of intact collagen fibrils. The large variability of C_R agrees well with the non-uniformity of STZ collagen density and AC

Table 2
Mean and standard deviation (SD) of parameter values and goodness of fit (R^2) for FJC, MAC, and TI models. The parameter C_R varied substantially for all three models, as indicated by its large SD in each case, while the remaining parameters displayed minimal variance. The TI model produced the best fit to the data based on its high R^2.

	FJC			MAC				TI				
	C_R[a]	N	R^2	C_R[a]	l_p[b]	L[b]	R^2	C_R[a]	a	b	J	R^2
Mean	113.34	1.048	0.995	3017.08	4.76	2.215	0.900	207.88	1.010	1.315	0.978	0.999
SD	106.94	0.014	0.003	3006.73	1.28	0.547	0.124	168.66	0.055	0.057	0.046	0.001

[a] In kilopascals (kPa).
[b] In millimeters.

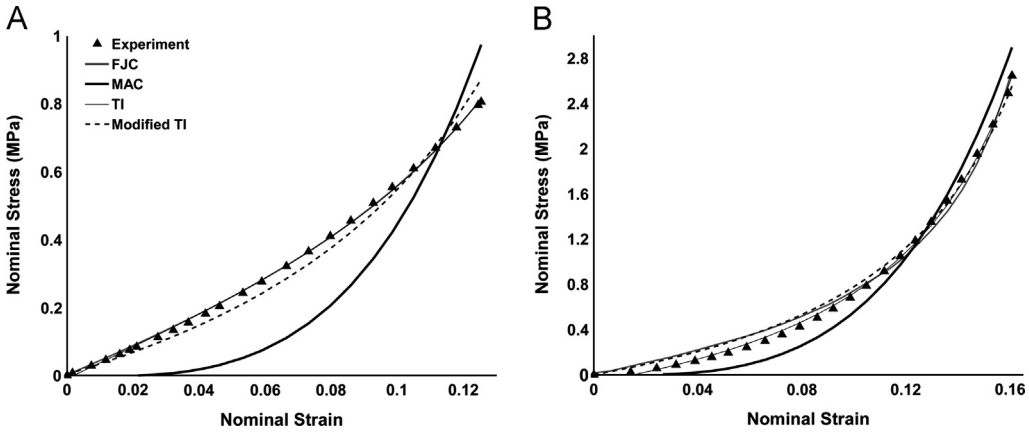

Fig. 5. Representative simulation results for the FJC, MAC, TI, and modified TI models for (A) nearly linear and (B) non-linear stress–strain responses. In Case A, the FJC and TI lines fall approximately on top of one another. In Case B, TI supplies a superior fit to FJC, particularly in the low-strain regime. The MAC model poorly fits the data in both situations.

Table 3
Mean C_R (kPa) for the TI model with $a=1$, $b=1.33$, and $J=1$ by knee (S_i, $i=1, 2,\ldots, 7$) and region (I-IV). Blank cells reflect missing data due to a lack of experimental data or a low R^2 of the simulation.

	Lateral plateau				Medial plateau				Both plateaus			
	I	II	III	IV	I	II	III	IV	I	II	III	IV
S_1	145.08	47.88	211.24	446.68	52.55	82.29	208.16	395.81	89.57	65.08	209.70	412.77
S_2		48.30	162.51	157.21	76.31	215.62	276.27	272.24	76.31	131.96	219.39	233.90
S_3	141.77	138.49	266.48	336.25	106.18	556.00	406.23	333.28	129.91	277.66	336.35	334.77
S_4		272.34	341.18	579.15		84.38	301.26	605.14		178.3	327.87	594.75
S_5	122.73	199.84	519.00	139.76	249.35	176.47	445.13	548.00	195.06	188.16	482.07	411.92
S_6	55.62	53.33	171.14	67.75	74.02		275.49	400.89	67.89	53.33	223.31	178.80
S_7	96.56	86.47	226.63	254.27	87.32		512.32	272.96	92.86	86.47	369.47	265.48

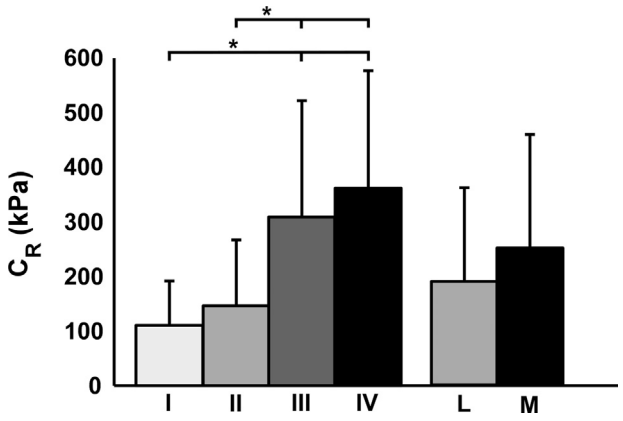

Fig. 6. Mean C_R of the modified TI simulations for the four regions (I–IV) and the lateral (L) and medial (M) plateaus. Bars represent 1 standard deviation. Asterisks (*) denote statistically significant differences ($p<0.05$). Statistically significant differences were determined between regions but not between the medial and lateral plateaus.

mechanical properties across the tibial plateau (Clark, 1991; Young et al., 2007). The central regions of the joint, which tend to experience compressive loading (Andriacchi et al., 2009; Bevill et al., 2008) and have a lower collagen density (Clark, 1991), also demonstrated lower mean C_R. In contrast, the posterior and lateral peripheral regions, which more frequently undergo shear loading (Andriacchi et al., 2009; Bevill et al., 2008) and have a higher collagen density (Clark, 1991), exhibited higher mean C_R. This suggests C_R as a useful parameter for incorporating regionally dependent mechanics (Deneweth et al., 2013).

The ratio a:b represents the degree of transverse isotropy in the tissue. The more the STZ collagen molecules align parallel to the surface, the greater the expected anisotropy. Meniscus-covered regions tend toward a higher density of parallel-aligned collagen compared to the meniscus-uncovered regions (Clark, 1991). In the present study, however, a:b remained relatively consistent across the tibial plateau. Considering the larger variability of C_R, this finding may indicate that collagen density rather than alignment contributes more to the unconfined compression response of the tissue. On average $b>a$, which is expected if the in-plane tensile

Table 4
Inter-region statistics for C_R (kPa) of the modified TI model with $a=1$, $b=1.33$, and $J=1$.

Regions		Lateral plateau					Medial plateau			
A	B	p[a]	Mean B–A[b]	95% CI[c]	Cohen's d	Effect size	Mean B–A[b]	95% CI[c]	Cohen's d	Effect size
I	II	1.000	8.82	(−48.92, 66.56)	0.12	Small	76.83	(−13.18, 166.84)	0.70	Moderate
I	III	0.004	159.04	(38.73, 279.34)	1.01	Strong	240.76	(141.36, 340.17)	1.74	Strong
I	IV	<0.001	176.09	(68.29, 283.89)	1.38	Strong	305.21	(199.09, 411.34)	2.02	Strong
II	III	0.038	155.22	(20.59, 279.85)	0.90	Strong	163.93	(7.38, 320.49)	0.95	Strong
II	IV	0.008	167.27	(47.77, 286.78)	1.20	Strong	228.38	(61.76, 395.00)	1.22	Strong
III	IV	1.00	−17.06	(−194.12, 160.01)	0.08	Weak	64.45	(−95.23, 224.13)	0.32	Small

[a] Bonferroni-corrected p-value for the pairwise comparison of mean C_R between Regions A and B. Both plateaus have been averaged for the comparison due to the lack of a statistically significant difference between them. $p<0.05$ denotes significance.
[b] Mean difference in C_R between Regions A and B.
[c] 95% confidence interval on the mean difference in C_R between Regions A and B.

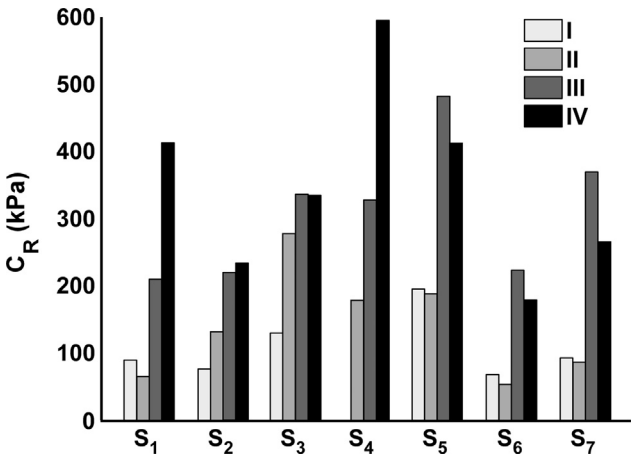

Fig. 7. Mean regional C_R of the modified TI simulations for each knee (S_i, $i=1, 2,\ldots, 7$). No data are available for Region I of S_4 because the R^2 value for this region fell below the pre-defined cut-off level of 0.97. Region values have been averaged across sides due to the lack of a statistically significant difference between the medial and lateral plateaus. The relative pattern of regional differences manifests similarly across the seven knees.

stiffness was greater than axial tensile stiffness. Lastly, J indicates the compressibility of the tissue. J remained nearly constant at 0.978, which agreed with expectations (Wong et al., 2000).

The TI model was successfully simplified to an incompressible model with a single material constant without compromising its ability to replicate tibial plateau AC mechanics. The material constant that remained, C_R, varied regionally in accordance with experimental findings (Deneweth et al., 2013). This suggested that regional mechanical dependence of the TI model can be established by representing the meniscus-uncovered, anterior meniscus-covered, and exterior-posterior meniscus-covered regions with separate C_R values while holding a,b, and J fixed. This represents a unique and powerful approach to modeling human cartilage: the constitutive relation is driven by the anisotropy and physiological variations (i.e., collagen density) of the superficial zone of the cartilage matrix, which makes the model highly applicable to the human knee joint. Since a regional shift in the joint loading pattern has been suggested to initiate knee osteoarthritis (Andriacchi et al., 2009), a tibial AC constitutive model that successfully captures regional stiffness variations could offer unique insight into the mechanisms of disease development over current models. Further, its ability to capture AC non-linearity with a single material constant is desirable for use in whole-joint computational models.

The TI model can be readily implemented into one of the many commercial finite element packages that permit user-defined hyperelastic materials. These routines typically require the model's strain energy, its derivatives, and parameter values. The TI strain energy is given in Eq. (9), with $b=c$, $\lambda_b=\lambda_c$, and $\alpha=1$. To model the heterogeneity in human cartilage, C_R (i.e., $nk\theta$) must be defined as a function of position across the cartilage surface, while J, a, and b can be assigned the values used in the second part of this study. An appropriate scenario for using the TI model is a material with known transverse anisotropy and a mechanical response that is largely dominated by non-linear, recoverable deformation.

The current study validated the models of interest with unconfined compression data. Future work must be done to determine whether the TI model can represent AC across the spectrum of potential deformation states. Additionally, the experimental data was taken from middle-aged Caucasian females, which prevents extrapolation to other populations.

Conflicts of interest

The authors have no conflicts of interest to report.

Acknowledgments

The authors gratefully acknowledge Ms. K. Newman, Ms. S. Pomeroy, and Mr. S. Sylvia for their assistance with data acquisition. Ms. Deneweth is supported by the Department of Defense through the National Defense Science & Engineering Graduate Fellowship Program.

References

Andriacchi, T.P., Koo, S., Scanlan, S.F., 2009. Gait mechanics influence healthy cartilage morphology and osteoarthritis of the knee. Journal of Bone and Joint Surgery American 91, 95–101.
Arruda, E.M., Boyce, M.C., 1993. A 3-dimensional constitutive model for the large stretch behavior of rubber elastic-materials. Journal of Mechanics and Physics of Solids 41, 389–412.
Askew, M.J., Mow, V.C., 1978. Biomechanical function of the collagen fibril ultrastructure of articular cartilage. Journal of Biomechanical Engineering 100, 105–115.
Ateshian, G.A., Ellis, B.J., Weiss, J.A., 2007. Equivalence between short-time biphasic and incompressible elastic material responses. Journal of Biomechanical Engineering 129, 405–412.
Bader, D.L., Kempson, G.E., 1994. The short-term compressive properties of adult human articular cartilage. Biomedical Materials and Engineering 4, 245–256.
Barker, M.K., Seedhom, B.B., 2001. The relationship of the compressive modulus of articular cartilage with its deformation response to cyclic loading: does cartilage optimize its modulus so as to minimize the strains arising in it due to the prevalent loading regime? Rheumatology 40, 274–284.
Bevill, S.L., Briant, P.L., Levenston, M.E., Andriacchi, T.P., 2008. Central and peripheral region tibial plateau chondrocytes respond differently to in vitro dynamic compression. Osteoarthritis and Cartilage 17, 980–987.

Bischoff, J.E., Arruda, E.M., Grosh, K., 2002. A microstructurally based orthotropic hyperelastic constitutive law. Journal of Applied Mechanics-T ASME 69, 570–579.
Bischoff, J.E., Arruda, E.M., Grosh, K., 2004. A rheological network model for the continuum anisotropic and viscoelastic behavior of soft tissue. Biomechanics and Modeling in Mechanobiology 3, 56–65.
Boschetti, F., Gervaso, F., Pennati, G., Peretti, G.M., Vena, P., Dubini, G., 2006. Poroelastic numerical modelling of natural and engineered cartilage based on in vitro tests. Biorheology 43, 235–247.
Boyce, M.C., Arruda, E.M., 2000. Constitutive models of rubber elasticity: a review. Rubber Chemistry and Technology 73, 504–523.
Boyce, M.C., Arruda, E.M., Jayachandran, R., 1994. The large-strain compression, tension, and simple shear of polycarbonate. Polymer Engineering and Science 34, 716–725.
Brown, C.P., Nguyen, T.C., Moody, H.R., Crawford, R.W., Oloyede, A., 2009. Assessment of common hyperelastic constitutive equations for describing normal and osteoarthritic articular cartilage. Proceedings of the Institution of Mechanical Engineers H 223, 643–652.
Buckwalter, J.A., Mankin, H.J., Grodzinsky, A.J., 2005. Articular cartilage and osteoarthritis. Instructional Course Lectures 54, 465–480.
Bullough, P., Goodfellow, J., 1968. The significance of the fine structure of articular cartilage. Journal of Bone and Joint Surgergy British 50, 852–857.
Chegini, S., Ferguson, S.J., 2010. Time and depth dependent Poisson's ratio of cartilage explained by an inhomogeneous orthotropic fiber embedded biphasic model. Journal of Biomechanics 43, 1660–1666.
Clark, J.M., 1991. Variation of collagen fiber alignment in a joint surface: a scanning electron microscope study of the tibial plateau in dog, rabbit, and man. Journal of Orthopaedic Research 9, 246–257.
Cohen, A., 1991. A Pade approximant to the inverse Langevin function. Rheologica Acta 30, 270–273.
Cohen, J., 1988. Statistical Power Analysis for the Behavioral Sciences. L. Erlbaum Associates, Hillsdale, N.J.
Coleman, T.F., Li, Y., 1996. An interior, trust region approach for nonlinear minimization subject to bounds. SIAM Journal of Optimization 6, 418–445.
Deneweth, J.M., Newman, K.E., Sylvia, S.M., McLean, S.G., Arruda, E.M., 2013. Heterogeneity of tibial plateau cartilage in response to a physiological compressive strain rate. Journal of Orthopaedic Research 31, 370–375.
Eyre, D.R., Weis, M.A., Wu, J.J., 2006. Articular cartilage collagen: an irreplaceable framework? European Cells and Materials 12, 57–63.
Hayes, W.C., Keer, L.M., Herrmann, G., Mockros, L.F., 1972. A mathematical analysis for indentation tests of articular cartilage. Journal of Biomechanics 5, 541–551.
Jurvelin, J.S., Buschmann, M.D., Hunziker, E.B., 2003. Mechanical anisotropy of the human knee articular cartilage in compression. Proceedings of the Institution of Mechanical Engineers H 217, 215–219.
Keenan, K.E., Pal, S., Lindsey, D.P., Besier, T.F., Beaupre, G.S. A viscoelastic constitutive model can accurately represent entire creep indentation tests of human patella cartilage. Journal of Applied Biomechanics, in press.
Korhonen, R.K., Laasanen, M.S., Toyras, J., Rieppo, J., Hirvonen, J., Helminen, H.J., Jurvelin, J.S., 2002. Comparison of the equilibrium response of articular cartilage in unconfined compression, confined compression and indentation. Journal of Biomechanics 35, 903–909.
Kühn, W., Grun, F., 1942. Relations between elastic constants and the strain birefringence of high-elastic substances. Kolloid-Zeitschrift 101, 248–271.
Lai, W.M., Hou, J.S., Mow, V.C., 1991. A triphasic theory for the swelling and deformation behaviors of articular cartilage. Journal of Biomechanical Engineering 113, 245–258.
Liu, F., Kozanek, M., Hosseini, A., Van de Velde, S.K., Gill, T.J., Rubash, H.E., Li, G., 2010. In vivo tibiofemoral cartilage deformation during the stance phase of gait. Journal of Biomechanics 43, 658–665.
Ma, J., Narayanan, H., Garikipati, K., Grosh, K., Arruda, E.M., 2010. Experimental and computational investigation of viscoelasticity of native and engineered ligament and tendon. IUTAM Symposium on Cellular, Molecular and Tissue Mechanics 16, pp. 3–17.
MacKintosh, F.C., Kas, J., Janmey, P.A., 1995. Elasticity of semiflexible biopolymer networks. Physical Review Letters 75, 4425–4428.
Mak, A.F., 1986. The apparent viscoelastic behavior of articular cartilage–the contributions from the intrinsic matrix viscoelasticity and interstitial fluid flows. Journal of Biomechanical Engineering 108, 123–130.
Maroudas, A.I., 1976. Balance between swelling pressure and collagen tension in normal and degenerate cartilage. Nature 260, 808–809.
Mizrahi, J., Maroudas, A., Lanir, Y., Ziv, I., Webber, T.J., 1986. The “instantaneous” deformation of cartilage: effects of collagen fiber orientation and osmotic stress. Biorheology 23, 311–330.
Mow, V.C., Holmes, M.H., Lai, W.M., 1984. Fluid transport and mechanical properties of articular cartilage: a review. Journal of Biomechanics 17, 377–394.
Mow, V.C., Kuei, S.C., Lai, W.M., Armstrong, C.G., 1980. Biphasic creep and stress relaxation of articular cartilage in compression? Theory and experiments. Journal of Biomechanical Engineering 102, 73–84.
Palmer, J.S., Boyce, M.C., 2008. Constitutive modeling of the stress–strain behavior of F-actin filament networks. Acta Biomaterialia 4, 597–612.
Poole, A.R., Kojima, T., Yasuda, T., Mwale, F., Kobayashi, M., Laverty, S., 2001. Composition and structure of articular cartilage: a template for tissue repair. Clinical Orthopaedics and Related Research (391 Suppl.), S26–33.
Shepherd, D.E., Seedhom, B.B., 1999. The ‘instantaneous' compressive modulus of human articular cartilage in joints of the lower limb. Rheumatology (Oxford) 38, 124–132.
Wang, C.C., Chahine, N.O., Hung, C.T., Ateshian, G.A., 2003. Optical determination of anisotropic material properties of bovine articular cartilage in compression. Journal of Biomechanics 36, 339–353.
Wilson, W., van Donkelaar, C.C., van Rietbergen, B., Ito, K., Huiskes, R., 2004. Stresses in the local collagen network of articular cartilage: a poroviscoelastic fibril-reinforced finite element study. Journal of Biomechanics 37, 357–366.
Wilson, W., van Donkelaar, C.C., van Rietbergen, R., Huiskes, R., 2005. The role of computational models in the search for the mechanical behavior and damage mechanisms of articular cartilage. Medical Engineering and Physics 27, 810–826.
Wong, M., Ponticiello, M., Kovanen, V., Jurvelin, J.S., 2000. Volumetric changes of articular cartilage during stress relaxation in unconfined compression. Journal of Biomechanics 33, 1049–1054.
Woo, S.L., Akeson, W.H., Jemmott, G.F., 1976. Measurements of nonhomogeneous, directional mechanical properties of articular cartilage in tension. Journal of Biomechanics 9, 785–791.
Young, A.A., Appleyard, R.C., Smith, M.M., Melrose, J., Little, C.B., 2007. Dynamic biomechanics correlate with histopathology in human tibial cartilage: a preliminary study. Clinical Orthopaedics and Related Research 462, 212–220.